HYDROGEN, FUEL CELL & ENERGY STORAGE

Thermodynamic and Thermoeconomic Analysis of a Multigeneration System Using Solar and Geothermal Energies

Shakir Mahmood Mejbel Ghrairi | Morteza Khalilian | Iraj Mirzaee*

Department of Mechanical Engineering, Engineering Faculty, Urmia University, Urmia, Iran
* Corresponding author, Email: i.mirzaee@urmia.ac.ir

Article Information

Article Type
Research Article

Article History
Received: *15 Aug 2024*
Revised: *16 Oct 2024*
Accepted: *11 Dec 2024*
Published Online: *04 Jan 2025*

Keywords

Multigeneration system
Solar energy
Geothermal energy
Hydrogen production
PEM electrolyzer

Abstract

Recently, discussions about energy and global warming have significantly increased the focus on renewable energy. One of the suitable options for this purpose is the use of multigeneration systems with solar and geothermal energy sources. In this research, a multigeneration system for hydrogen, cooling, heating and power production based on the organic Rankine cycle, absorption chiller cycle dryer, and the proton exchange membrane (PEM) electrolyzer is investigated from thermodynamic and thermoeconomic points of view. In the organic Rankine cycles (ORC), a thermoelectric generator (TEG) unit is applied instead of a condenser, and different working fluids are tested to study their performance on the system. All the simulations are carried out using the Engineering Equation Solver (EES) software. The impact of different factors on the efficiency of the multigeneration system is investigated. The system's energetic efficiency is measured at 41.58%, while its exergetic efficiency stands at 25.61%, according to the findings. Moreover, by using the TEG unit, 466.4 kW extra power is obtained. Furthermore, the system can generate 493.1 kg/day hydrogen. From an exergy destruction perspective, the solar collector and the PEM electrolyzer exhibit the highest amounts. Finally, it is demonstrated that the geothermal temperature and turbine inlet temperature positively impact the system's performance, while collector inlet temperature leads to a decrease in performance.

Cite this article: Ghrairi, S. M. M., Khalilian, M., Mirzaee, I. (2025). Thermodynamic and Thermoeconomic Analysis of a Multigeneration System Using Solar and Geothermal Energies. DOI: 10.22104/hfe.2024.6923.1301

Publisher: Iranian Research Organization for Science and Technology (IROST)
DOI: 10.22104/hfe.2024.6923.1301

1 Introduction

Multigeneration systems refer to systems that produce more than three outputs [1]. In addition to generating power, cooling and heating, these systems can also facilitate several other energetic processes, such as the production of chemicals, hydrogen, ethanol, biodiesel, fertilizers, and drinking water. These systems are utilized in power plants or units with high energy demand. It should be noted that the design of these systems is tailored to their specific application and location requirements. These systems are also proposed as a solution to mitigate global warming, which is one of the fundamental challenges of the last century. The Rankine cycle is utilized to generate power within these systems. The absorption refrigeration system is employed to provide cooling, utilizing waste heat from this system to produce fresh water. Additionally, the electrolyzer is used to generate hydrogen, with the system supplying the necessary power for water electrolysis. Indeed, hydrogen production serves as a method to store the system's generated power during the day for use at night when sunlight is insufficient. Multigeneration systems offer benefits such as improved energy efficiency, reduced heat losses, lower operational expenses, minimized greenhouse gas emissions, enhanced resource utilization, increased dependability, and decreased network losses. These systems enhance the overall efficiency of the unit while lowering operating costs. In conventional power plants using fossil fuels, energy efficiency is typically less than 40%, with heat losses exceeding 60%. However, in conventional power plants that simultaneously produce electricity and heat, energy efficiency can reach about 60%. In contrast, multigeneration systems, utilizing waste heat, can achieve efficiencies of up to 80% [2, 3]. In power plants employing multigeneration systems, unlike conventional power plants, waste heat from electricity production is utilized for heating and cooling units, eliminating the need for additional fuel. Consequently, multigeneration systems exhibit lower energy consumption and operating costs compared to conventional systems when generating the same products. As mentioned, due to reduced fuel consumption for producing the same products, multigeneration systems emit fewer greenhouse gases compared to conventional systems.

Choosing the most suitable energy source is crucial for a sustainable energy system. Several key criteria must be considered when selecting the right energy source [4]. Among these criteria, we can mention abundance, local availability, reasonable price, reliability, safety and compatibility with the environment. Solar energy is the primary source among renewable energies, as it is the fundamental driver of natural cycles related to other renewables such as wind, water, biomass and ocean. Converting solar energy into desired forms of energy using suitable equipment is desirable [5]. Solar radiation concentrating collectors, such as solar towers with heliostat fields and parabolic collectors such as solar dishes, are typically utilized for thermodynamic cycles in power generation and heat engines such as Stirling engines, owing to the high temperatures they can achieve [6, 7]. Due to the advantages of the multigeneration systems, they have garnered the attention of many researchers. Various types of prime movers can be utilized in these systems. In their study, Tashtoush et al. [8] used the Transient System Simulation Tool (TRNSYS) software to evaluate the transient performance of a 7 kW solar ejector cooling system utilizing R134a as the refrigerant. During peak solar radiation and the highest ambient temperature, the system achieved an overall efficiency of at least 0.32. The efficiency of the solar collector ranged from 0.52 to 0.92, while the overall efficiency varied between 0.32 and 0.47.

Yilmaz [9] conducted research on the thermodynamic performance of a recently developed cogeneration system utilizing solar energy. The system was designed to generate hydrogen, electricity, heat, cooling, and potable water. The findings revealed that the system achieved an overall energy efficiency of 78.93% and an exergy efficiency of 47.56%. Furthermore, the system produced hydrogen at a rate of 0.04663 kg/s and fresh water at a rate of 0.882 kg/s. Islam et al. [10] conducted a study comparing the energy and exergy aspects of a multigeneration system with two different setups. One setup combined the output of thermal generators with parabolic solar collectors, while the other setup incorporated thermoelectric generators between the solar heat exchanger and the first organic Rankine cycle. The incorporation of thermoelectric devices in the second arrangement enhances the energy and overall efficiency of both the multigeneration system and the initial organic Rankine cycle. Additionally, the first organic Rankine cycle in system 2 experienced a significant improvement in the amount of net work produced. The findings indicated that increasing the mass flow rate of solar heat transfer fluid notably enhances the output of turbines and thermoelectric generators.

In their study, Colakoglu and Durmayaz [11] developed a solar gas turbine-based multigeneration system and conducted multi-objective optimization considering energy, exergy, and environmental aspects. This system integrated a gas turbine cycle with a solar tower axis, a Kalina cycle, an organic Rankine cycle, a single effect absorption refrigeration cycle, an electrolyzer, and two domestic water heaters. The results indicated

that the proposed system achieved energy and exergy efficiencies of 55.57% and 39.45%, respectively.

Haghighi et al. [12] conducted a thermodynamic assessment of a multigeneration system that includes electrical energy, cooling, drinking water, sanitary water, and hydrogen. The system is based on a solid oxide fuel cell and incorporates a gas turbine, a biomass combustion subsystem, an organic Rankine cycle, an ejector refrigeration cycle, a desalination subsystem, and an electrolysis subsystem. Under standard design conditions, the system demonstrated a net electrical power of 4392 kW, a cooling load of 164.2 kW, and achieved total energy and exergy efficiencies of 77.58% and 47.14%, respectively. Furthermore, the production rates for drinking and sanitary water and hydrogen were 53.27, 52.50, and 0.7695 moles per second, respectively.

In their study, Cioccolanti et al. [13] conducted a life cycle assessment of a small-scale cogeneration power plant. The plant included a 50 square meter parabolic collector solar field, a 3 cubic meter oil storage tank, a 3.5 kW organic Rankine power plant, and a 17 kW absorption chiller. Their research indicated that selecting the appropriate working fluid and solar field size can significantly optimize the power plant. The system's outputs are limited to heating, cooling, and electrical power.

In their study, Saleem et al. [14] used TRYNSYS software to model an energy system. They evaluated 15 different working fluids and used REFPROP software to calculate their chemical properties. The findings indicated that ammonia provides the highest energy yield. Additionally, the research suggests that in large-scale energy systems, using batteries for energy storage may be limited due to significant limitations. To enhance overall efficiency, integrating a refrigeration unit into the co-production system would be more advantageous.

To validatethe simulation of a new power plant model, Uche et al. [15] conducted experimental tests on a small multigeneration unit utilizing renewable energies. The system generated electricity through solar photovoltaics and a wind turbine, produced fresh water through desalination, and provided sanitary hot water using solar collectors. This power plant was engineered specifically for off-grid operation and utilized traditional energy storage systems.

Sohani et al [16] conducted research to determine the optimal operating conditions for a Solar-Geothermal Multigeneration System, capable of simultaneously generating hydrogen, fresh water, electricity, and heat. The study reported a 14.4% increase in annual electricity production, a 16.1% increase in heat production, a 13.5% increase in hydrogen production, and a 14.3% increase in fresh water production. Additionally, the average annual exergy efficiency improved by 5.2% and energy efficiency by 3.0%.

Upon investigating the previous studies, it was noted that most of them utilized only one ORC cycle, with TEG applications being rare. Therefore, in this study, two ORC systems and two TEG units are employed to generate additional power. This system's novelty lies in replacing two ORC condensers with two TEG units to produce extra electricity.

2 System Description

Solar energy and geothermal energy are the primary renewable energy sources for the proposed multigeneration system. The system integrates two organic Rankine cycles (ORC) for power generation, a single-effect absorption refrigeration cycle for cooling, a heat exchanger for heat production and dry air for product drying, and a Proton Exchange Membrane (PEM) electrolyzer for hydrogen production. Solar energy powers one of the ORCs, while geothermal energy powers the other. Additionally, geothermal energy is enhanced by utilizing solar energy for additional heating. It is noteworthy that in ORC cycles, a Thermoelectric Generator (TEG) unit is utilized instead of condensers to generate additional power. A detailed illustration of the analyzed system can be found in Figure 1.

In one phase of the process, the Therminol VP1 working fluid is heated by solar energy as it passes through the solar collector. Subsequently, it moves into the steam generator and economizer of the ORC cycle, where it transfers its heat to the n-pentane working fluid of the organic Rankine cycle. The n-pentane fluid undergoes work in the ORC turbine, converting it into electricity through the power generator. As a result, it meets the necessary cooling demands via the absorption chiller cycle. In the second part of the system, the geothermal fluid is heated using solar energy, and then it enters the superheater of another ORC cycle to generate power with the ORC turbine. The power generated by the ORC turbines and the TEG units is used for residential buildings and for hydrogen production in the PEM electrolyzer. Dry and hot air, heated by the solar working fluid, is employed in the dryer to dehydrate a moist product.

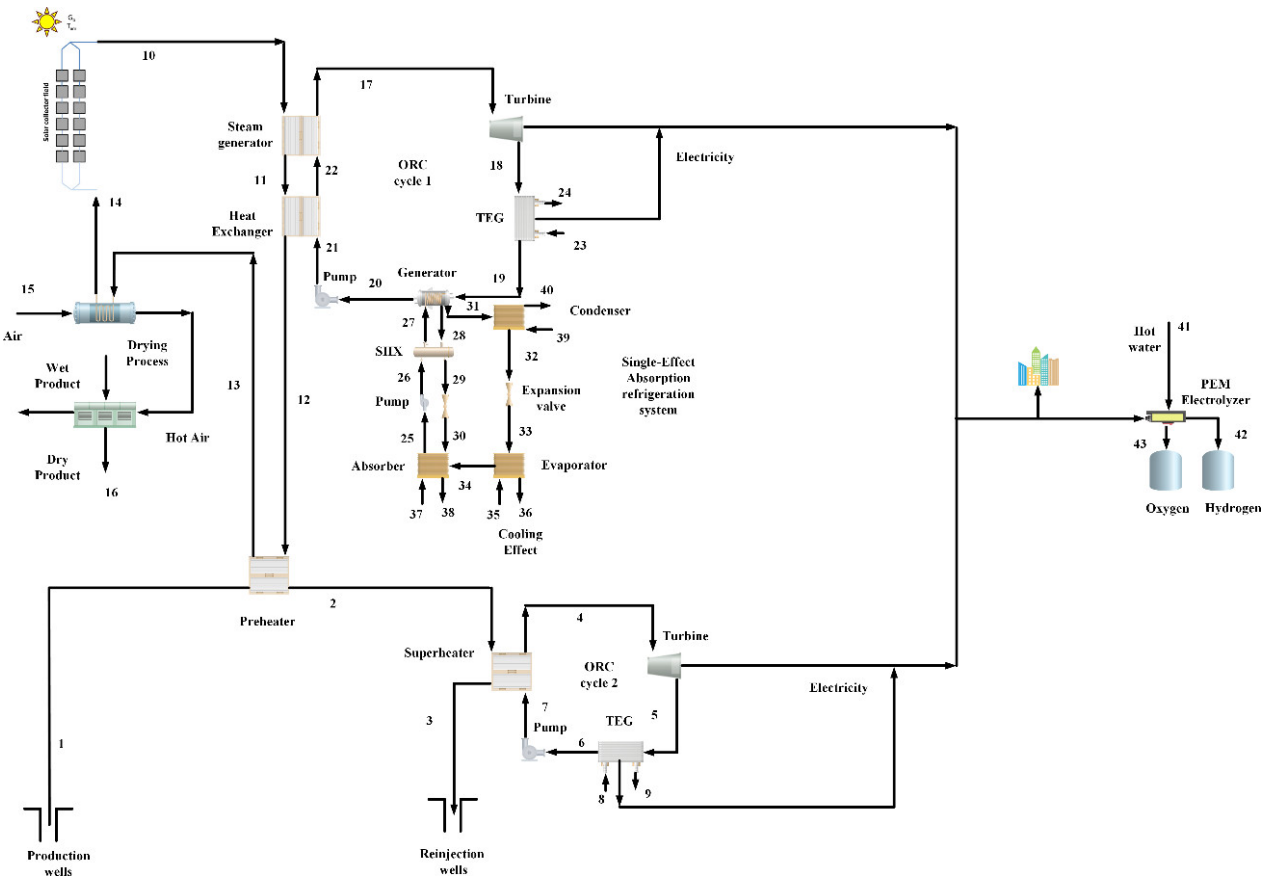

Fig. 1. The integrated multigeneration system is depicted in the schematic, which combines solar and geothermal energy sources.

The system uses the following basic equations for conducting thermodynamic analysis [17].

$$\sum \dot{m}_{\text{in}} - \sum \dot{m}_{\text{out}} = \frac{dm_{\text{cv}}}{dt}\,, \tag{1}$$

$$\dot{Q} - \dot{W} + \sum_{\text{in}} \dot{m}_{\text{in}}\left(h_{\text{in}} + \frac{V_{\text{in}}^2}{2} + gZ_{\text{in}}\right) - \sum_{\text{out}} \dot{m}_{\text{out}}\left(h_{\text{out}} + \frac{V_{\text{out}}^2}{2} + gZ_{\text{out}}\right) = \frac{dE_{\text{cv}}}{dt}\,, \tag{2}$$

$$\dot{\text{E}}\text{x}_Q + \sum_{\text{in}} \dot{m}_{\text{in}}\text{ex}_{\text{in}} = \sum_{\text{out}} \dot{m}_{\text{out}}\text{ex}_{\text{out}} + \dot{\text{E}}\text{x}_W + \dot{\text{E}}\text{x}_D\,, \tag{3}$$

$$\dot{\text{E}}\text{x}_{\text{ph}} = \sum \dot{m}_{\text{in}}\left[(h_{\text{in}} - h_{\text{out}}) - T_0(s_{\text{in}} - s_{\text{out}})\right]. \tag{4}$$

In an economic analysis, the entire system's cost balance is expressed as shown in reference [18].

$$\dot{C}_{p,\text{tot}} = \dot{C}_{F,\text{tot}} + \dot{Z}_{\text{tot}}^{\text{CI}} + \dot{Z}_{\text{tot}}^{\text{O\&M}}\,, \tag{5}$$

The cost balance indicates that the product cost rate of system ($\dot{C}_{p,\text{tot}}$) is equal to the sum of the fuel cost rate ($\dot{C}_{F,\text{tot}}$), the initial capital investment cost rate ($\dot{Z}_{\text{tot}}^{\text{CI}}$), and the operating and maintenance cost rate ($\dot{Z}_{\text{tot}}^{\text{O\&M}}$). The cost rate of each component is [19]:

$$\dot{Z}_k = \frac{Z_k\,\varphi\,\text{CRF}}{\tau}\,, \tag{6}$$

in which Z_k shows the cost per component, φ represents the maintenance factor and its amount is 1.06. N is the number of operating hours of the system. Capital recovery factor is described as:

$$\text{CRF} = \frac{i_r(1+i_r)^n}{(1+i_r)^n - 1}\,. \tag{7}$$

In this equation i and n show the interest rate and the lifetime of the system, respectively, and are equal to 0.1 and 20 [20]. The collector yields power that is valuable and equivalent to:

$$Q_u = n_{cp}n_{cs}F_R A_{\text{ap}}\left[S - \frac{A_r}{A_{\text{ap}}}U_L(T_{r,i} - T_0)\right]. \tag{8}$$

The equation above is employed to determine the exergy of the solar collector.

$$\dot{\text{E}}\text{x}_s = A_{\text{ap}}G_b\left[1 + \frac{1}{3}\left(\frac{T_0}{T_s}\right)^4 - \frac{4}{3}\left(\frac{T_0}{T_s}\right)\right]. \tag{9}$$

The formula below can be used to calculate the power produced by the TEG unit.

$$\dot{W}_{\mathrm{TEG}} = \eta_{\mathrm{TEG}}\, \dot{Q}_{\mathrm{cold}}\,, \tag{10}$$

$$\eta_{\mathrm{TEG}} = \eta_{\mathrm{Carnot}} \left[\frac{(1+\mathrm{ZT}_m)^{0.5} - 1}{(1+\mathrm{ZT}_m)^{0.5} - \left(\frac{T_{\mathrm{cold}}}{T_{\mathrm{hot}}}\right)} \right] \tag{11}$$

$$\mathrm{ZT}_m = \frac{S^2 \sigma T}{K_{\mathrm{tot}}}\,. \tag{12}$$

The thermodynamic equations for the different parts of the multigeneration system are listed in Table 1.

Table 1. The proposed system's energy balance equations and exergy destruction rate for each component need to be determined.

Component	Energy balance equations	Exergy destruction rate equations
PTC collector	$\dot{m}_{14}h_{14} + \dot{Q}_u = \dot{m}_{10}h_{10}$	$\dot{\mathrm{E}}\mathrm{x}_{D,\mathrm{PTC}} = \dot{\mathrm{E}}\mathrm{x}_{\mathrm{sun}} + \dot{\mathrm{E}}\mathrm{x}_{14} - \dot{\mathrm{E}}\mathrm{x}_{10}$
ORC steam generator	$\dot{Q}_{\mathrm{sg,ORC}} = \dot{m}_{10}(h_{10} - h_{11} = \dot{m}_{17}(h_{17} - h_{22})$	$\dot{\mathrm{E}}\mathrm{x}_{d,\mathrm{sg,ORC}} = \dot{\mathrm{E}}\mathrm{x}_{10} + \dot{\mathrm{E}}\mathrm{x}_{22} - \dot{\mathrm{E}}\mathrm{x}_{11} - \dot{\mathrm{E}}\mathrm{x}_{17}$
ORC Economizer	$\dot{Q}_{\mathrm{eco,ORC}} = \dot{m}_{11}(h_{11} - h_{12} = \dot{m}_{21}(h_{22} - h_{21})$	$\dot{\mathrm{E}}\mathrm{x}_{d,\mathrm{eco,ORC}} = \dot{\mathrm{E}}\mathrm{x}_{11} + \dot{\mathrm{E}}\mathrm{x}_{21} - \dot{\mathrm{E}}\mathrm{x}_{12} - \dot{\mathrm{E}}\mathrm{x}_{22}$
ORC1 turbine	$\dot{W}_{t,\mathrm{ORC1}} = \dot{m}_{17}(h_{17} - h_{18})$	$\dot{\mathrm{E}}\mathrm{x}_{D,t,\mathrm{ORC1}} = \dot{\mathrm{E}}\mathrm{x}_{17} - \dot{W}_{t,\mathrm{ORC1}} - \dot{\mathrm{E}}\mathrm{x}_{18}$
ORC2 turbine	$\dot{W}_{t,\mathrm{ORC2}} = \dot{m}_{4}(h_{4} - h_{5})$	$\dot{\mathrm{E}}\mathrm{x}_{D,t,\mathrm{ORC2}} = \dot{\mathrm{E}}\mathrm{x}_{4} - \dot{W}_{t,\mathrm{ORC2}} - \dot{\mathrm{E}}\mathrm{x}_{5}$
ORC1 TEG	$\dot{Q}_{\mathrm{TEG,ORC1}} = \dot{m}_{18}(h_{18} - h_{19}) = \dot{m}_{23}(h_{24} - h_{23})$	$\dot{\mathrm{E}}\mathrm{x}_{D,\mathrm{TEG,ORC1}} = \dot{\mathrm{E}}\mathrm{x}_{18} + \dot{\mathrm{E}}\mathrm{x}_{23} - \dot{\mathrm{E}}\mathrm{x}_{19} - \dot{\mathrm{E}}\mathrm{x}_{24}$
ORC2 TEG	$\dot{Q}_{\mathrm{TEG,ORC2}} = \dot{m}_{5}(h_{5} - h_{6}) = \dot{m}_{8}(h_{9} - h_{8})$	$\dot{\mathrm{E}}\mathrm{x}_{D,\mathrm{TEG,ORC2}} = \dot{\mathrm{E}}\mathrm{x}_{5} + \dot{\mathrm{E}}\mathrm{x}_{8} - \dot{\mathrm{E}}\mathrm{x}_{6} - \dot{\mathrm{E}}\mathrm{x}_{9}$
ORC1 pump	$\dot{W}_{p,\mathrm{ORC1}} = \dot{m}_{20}(h_{21} - h_{20})$	$\dot{\mathrm{E}}\mathrm{x}_{D,p,\mathrm{ORC1}} = \dot{W}_{p,\mathrm{ORC1}} - \dot{\mathrm{E}}\mathrm{x}_{20} + \dot{\mathrm{E}}\mathrm{x}_{21}$
ORC2 pump	$\dot{W}_{p,\mathrm{ORC2}} = \dot{m}_{6}(h_{7} - h_{6})$	$\dot{\mathrm{E}}\mathrm{x}_{D,p,\mathrm{ORC2}} = \dot{W}_{p,\mathrm{ORC2}} - \dot{\mathrm{E}}\mathrm{x}_{6} + \dot{\mathrm{E}}\mathrm{x}_{7}$
SEARC-Generator	$\dot{Q}_{\mathrm{gen,SEARC2}} = \dot{m}_{19}(h_{19} - h_{20})$	$\dot{\mathrm{E}}\mathrm{x}_{d,\mathrm{gen,SEARC}} = \dot{\mathrm{E}}\mathrm{x}_{19} + \dot{\mathrm{E}}\mathrm{x}_{27} - \dot{\mathrm{E}}\mathrm{x}_{20} - \dot{\mathrm{E}}\mathrm{x}_{28} - \dot{\mathrm{E}}\mathrm{x}_{31}$
SEARC-Condenser	$\dot{Q}_{\mathrm{cond,SEARC}} = \dot{m}_{31}(h_{31} - h_{32}) = \dot{m}_{39}(h_{40} - h_{39})$	$\dot{\mathrm{E}}\mathrm{x}_{d,\mathrm{cond,SEARC}} = \dot{\mathrm{E}}\mathrm{x}_{31} + \dot{\mathrm{E}}\mathrm{x}_{39} - \dot{\mathrm{E}}\mathrm{x}_{32} - \dot{\mathrm{E}}\mathrm{x}_{40}$
SEARC-Solution heat exchanger	$\dot{Q}_{\mathrm{SHX,DEARC}} = \dot{m}_{28}(h_{28} - h_{29}) = \dot{m}_{26}(h_{27} - h_{26})$	$\dot{\mathrm{E}}\mathrm{x}_{d,\mathrm{SHX,SEARC}} = \dot{\mathrm{E}}\mathrm{x}_{28} + \dot{\mathrm{E}}\mathrm{x}_{26} - \dot{\mathrm{E}}\mathrm{x}_{29} - \dot{\mathrm{E}}\mathrm{x}_{27}$
SEARC-Evaporator	$\dot{Q}_{\mathrm{eva,SEARC}} = \dot{m}_{33}(h_{34} - h_{33}) = \dot{m}_{35}(h_{36} - h_{35})$	$\dot{\mathrm{E}}\mathrm{x}_{d,\mathrm{eva,SEARC}} = \dot{\mathrm{E}}\mathrm{x}_{33} + \dot{\mathrm{E}}\mathrm{x}_{35} - \dot{\mathrm{E}}\mathrm{x}_{34} - \dot{\mathrm{E}}\mathrm{x}_{36}$
SEARC-Absorber	$\dot{Q}_{\mathrm{abs,SEARC}} = \dot{m}_{30}h_{30} + \dot{m}_{34}h_{34} - \dot{m}_{25}h_{25} = \dot{m}_{37}(h_{38} - h_{37})$	$\dot{\mathrm{E}}\mathrm{x}_{d,\mathrm{abs,SEARC}} = \dot{\mathrm{E}}\mathrm{x}_{30} + \dot{\mathrm{E}}\mathrm{x}_{34} + \dot{\mathrm{E}}\mathrm{x}_{37} - \dot{\mathrm{E}}\mathrm{x}_{25} - \dot{\mathrm{E}}\mathrm{x}_{38}$
SEARC-Pump	$\dot{W}_{p,\mathrm{SEARC}} = \dot{m}_{25}(h_{26} - h_{25})$	$\dot{\mathrm{E}}\mathrm{x}_{d,p,\mathrm{SEARC}} = \dot{W}_{p,\mathrm{DEARC}} + \dot{\mathrm{E}}\mathrm{x}_{25} - \dot{\mathrm{E}}\mathrm{x}_{26}$
PEM	$\dot{W}_{\mathrm{PEM}} = \dot{m}_{41}h_{41} - \dot{m}_{42}h_{42} - \dot{m}_{43}h_{43}$	$\dot{\mathrm{E}}\mathrm{x}_{D,\mathrm{PEM}} = \dot{\mathrm{E}}\mathrm{x}_{41} + \dot{W}_{\mathrm{PEM}} - \dot{\mathrm{E}}\mathrm{x}_{42} - \dot{\mathrm{E}}\mathrm{x}_{43}$
Preheater	$\dot{Q}_{\mathrm{ph}} = \dot{m}_{12}(h_{12} - h_{13}) = \dot{m}_{1}(h_{2} - h_{1})$	$\dot{\mathrm{E}}\mathrm{x}_{\mathrm{ph}} = \dot{\mathrm{E}}\mathrm{x}_{1} + \dot{\mathrm{E}}\mathrm{x}_{12} - \dot{\mathrm{E}}\mathrm{x}_{2} - \dot{\mathrm{E}}\mathrm{x}_{13}$
Drying process	$(\dot{m}_{\mathrm{air}}h_{\mathrm{air}})_{\mathrm{in}} + (\dot{m}_{\mathrm{prod}}h_{\mathrm{prod}})_{\mathrm{in}} + (\dot{m}_{\mathrm{water}}h_{\mathrm{water}})_{\mathrm{in}} = (\dot{m}_{\mathrm{air}}h_{\mathrm{air}})_{\mathrm{out}} + (\dot{m}_{\mathrm{prod}}h_{\mathrm{prod}})_{\mathrm{out}} + (\dot{m}_{\mathrm{water}}h_{\mathrm{water}})_{\mathrm{out}} + \dot{Q}_{\mathrm{loss}}$	$\dot{\mathrm{E}}\mathrm{x}_{d,\mathrm{dry}} = (\dot{m}_{\mathrm{air}}\mathrm{ex}_{\mathrm{air}})_{\mathrm{in}} + (\dot{m}_{\mathrm{prod}}\mathrm{ex}_{\mathrm{prod}})_{\mathrm{in}} + (\dot{m}_{\mathrm{water}}\mathrm{ex}_{\mathrm{water}})_{\mathrm{in}} - (\dot{m}_{\mathrm{air}}\mathrm{ex}_{\mathrm{air}})_{\mathrm{out}} - (\dot{m}_{\mathrm{prod}}\mathrm{ex}_{\mathrm{prod}})_{\mathrm{out}} - (\dot{m}_{\mathrm{water}}\mathrm{ex}_{\mathrm{water}})_{\mathrm{out}} + \dot{Q}_{\mathrm{loss}}(1 - \frac{T_0}{T_{\mathrm{avg}}})$
$\mathrm{COP}_{\mathrm{en}}$	$\mathrm{COP}_{\mathrm{en}} = \dfrac{\dot{Q}_{\mathrm{eva,SEARC}}}{\dot{Q}_{\mathrm{gen,SEARC}} + \dot{W}_{\mathrm{net,SEARC}}}$	
$\mathrm{COP}_{\mathrm{ex}}$	$\mathrm{COP}_{\mathrm{ex}} = \dfrac{\dot{Q}_{\mathrm{eva,SEARC}}(1 - \frac{T_0}{T_{\mathrm{eva}}})}{\dot{Q}_{\mathrm{gen,SEARC}}(1 - \frac{T_0}{T_{\mathrm{gen}}}) + \dot{W}_{\mathrm{net,SEARC}}}$	
Thermal efficiency	$\eta_{\mathrm{th,tot}} = \dfrac{\dot{W}_{\mathrm{net}} + \dot{Q}_{\mathrm{cooling}} + \dot{m}_{42}\mathrm{HHV}_{\mathrm{H2}} - \dot{W}_{\mathrm{PEM}}}{\dot{Q}_u + \dot{m}_1 h_1}$	
Exergy efficiency	$\eta_{\mathrm{ex,tot}} = \dfrac{\dot{W}_{\mathrm{net}} + \dot{\mathrm{E}}\mathrm{x}_{\mathrm{cooling}} + \dot{\mathrm{E}}\mathrm{x}_{42} + \dot{\mathrm{E}}\mathrm{x}_{43}}{\dot{\mathrm{E}}\mathrm{x}_{\mathrm{in,sun}} + \dot{\mathrm{E}}\mathrm{x}_{1}}$	

Additionally, Table 2 presents the essential equations for analyzing the system's cost functions.

Table 2. Cost functions for each system component [21–23].

Component	Purchase cost ($)
PTC Solar collector	$Z_{\mathrm{PTC}} = 240A_{\mathrm{ap}}$
Heat exchangers	$Z_{\mathrm{HX}} = 130(\frac{A}{0.093})^{0.78}$
Preheater	$Z_{\mathrm{ph}} = 1397(A_{\mathrm{ph}})^{0.89}$
Turbine	$Z_t = 4405(\dot{W}_t)^{0.7}$
Pump	$Z_p = 1120(\dot{W}_p)^{0.8}$
Expansion valve	$Z_{\mathrm{exv}} = 114.5\dot{m}_{\mathrm{exv}}$
Generator	$Z_{\mathrm{des}} = 17500(A_{\mathrm{des}})^{0.514}$
Condenser	$Z_{\mathrm{cond}} = 1773\dot{m}_{\mathrm{cond}}$
TEG	$Z_{\mathrm{TEG}} = 1500\dot{W}_{\mathrm{TEG}}$
PEM	$Z_{\mathrm{PEM}} = 1000\dot{W}_{\mathrm{PEM}}$

Table 3 provides the cost balance equations and auxiliary equations for calculating the cost rate of exergy flows and the exergy unit price of each flow.

3 Results and Discussion

The system simulation is based on the following assumptions:

1. The proposed systemis expected to operate under constant conditions.
2. The assumption is that there is no pressure drop across the evaporator, condenser, and all heat exchangers.
3. The condenser's output fluid is assumed to be in the saturated liquid state.
4. It is assumed that the efficiency of the pump and turbine is isentropic.
5. All components studied in the system are treated as control volumes.
6. Air is assumed to behave asan ideal gas.
7. The geothermal working fluid is assumed to be water.
8. Solar radiation is assumed to be uniform and steady-state.

Table 3. Cost balance relations and deriving auxiliary equations for each component of the system.

Component	Cost balance equation	Auxiliary equation
PTC Solar collector	$\dot{C}_{\mathrm{sun}} + \dot{C}_{14} + \dot{Z}_{\mathrm{PTC}} = \dot{C}_{10}$	$c_{14} = c_{10}\,,\ c_{\mathrm{sun}} = 0$
Steam generator	$\dot{C}_{10} + \dot{C}_{22} + \dot{Z}_{\mathrm{sg,ORC}} = \dot{C}_{11} + \dot{C}_{17}$	$c_{10} = c_{11}$
Economizer	$\dot{C}_{11} + \dot{C}_{21} + \dot{Z}_{\mathrm{eco,ORC}} = \dot{C}_{12} + \dot{C}_{21}$	$c_{11} = c_{12}$
Preheater	$\dot{C}_{12} + \dot{C}_{1} + \dot{Z}_{\mathrm{ph}} = \dot{C}_{13} + \dot{C}_{2}$	$c_{12} = c_{13}$
ORC1 turbine	$\dot{C}_{17} + \dot{Z}_{t,\mathrm{ORC1}} = \dot{C}_{18} + \dot{C}_{w,t,\mathrm{ORC}}$	$c_{17} = c_{18}$
ORC2 turbine	$\dot{C}_{4} + \dot{Z}_{t,\mathrm{ORC2}} = \dot{C}_{5} + \dot{C}_{w,t,\mathrm{ORC}}$	$c_{4} = c_{5}$
ORC1 TEG	$\dot{C}_{18} + \dot{C}_{23} + \dot{Z}_{\mathrm{TEG1}} = \dot{C}_{19} + \dot{C}_{24}$	$c_{18} = c_{19},\ c_{23} = 0$
ORC2 TEG	$\dot{C}_{5} + \dot{C}_{8} + \dot{Z}_{\mathrm{TEG2}} = \dot{C}_{6} + \dot{C}_{9}$	$c_{5} = c_{6},\ c_{8} = 0$
ORC1 pump	$\dot{C}_{21} = \dot{Z}_{p,\mathrm{ORC1}} + \dot{C}_{20} + \dot{C}_{w,p,\mathrm{ORC}}$	$c_{w,p,\mathrm{ORC}} = c_{w,t,\mathrm{ORC}}$
ORC2 pump	$\dot{C}_{7} = \dot{Z}_{p,\mathrm{ORC2}} + \dot{C}_{6} + \dot{C}_{w,p,\mathrm{ORC}}$	$c_{w,p,\mathrm{ORC}} = c_{w,t,\mathrm{ORC}}$
SEARC-Generator	$\dot{C}_{19} + \dot{C}_{27} + \dot{Z}_{\mathrm{gen,SEARC}} = \dot{C}_{20} + \dot{C}_{28} + \dot{C}_{31}$	$c_{19} = c_{20}\,,\ \frac{\dot{C}_{28} - \dot{C}_{27}}{\dot{\mathrm{E}}\mathrm{x}_{28} - \dot{\mathrm{E}}\mathrm{x}_{27}} = \frac{\dot{C}_{31} - \dot{C}_{27}}{\dot{\mathrm{E}}\mathrm{x}_{31} - \dot{\mathrm{E}}\mathrm{x}_{27}}$
SEARC-Condenser	$\dot{C}_{31} + \dot{C}_{39} + \dot{Z}_{\mathrm{cond,SEARC}} = \dot{C}_{32} + \dot{C}_{40}$	$c_{31} = c_{32},\ c_{39} = 0$
SEARC-Evaporator	$\dot{C}_{33} + \dot{C}_{35} + \dot{Z}_{\mathrm{eva,SEARC}} = \dot{C}_{34} + \dot{C}_{36}$	$c_{33} = c_{34},\ c_{35} = 0$
SEARC-Absorber	$\dot{C}_{30} + \dot{C}_{34} + \dot{C}_{37} + \dot{Z}_{\mathrm{abs,SEARC}} = \dot{C}_{25} + \dot{C}_{38} + \dot{C}_{31}$	$c_{37} = 0\,,\ \frac{\dot{C}_{30} + \dot{C}_{34}}{\dot{\mathrm{E}}\mathrm{x}_{30} + \dot{\mathrm{E}}\mathrm{x}_{34}} = c_{25}$
SEARC-SHX	$\dot{C}_{26} + \dot{C}_{28} + \dot{Z}_{\mathrm{SHX,SEARC}} = \dot{C}_{27} + \dot{C}_{29}$	$c_{28} = c_{29}$
SEARC-Pump	$\dot{C}_{26} = \dot{Z}_{p,\mathrm{SEARC}} + \dot{C}_{25} + \dot{C}_{w,p,\mathrm{ORC}}$	$c_{w,p,\mathrm{DEARC}} = c_{w,t,\mathrm{ORC}}$
PEM	$\dot{C}_{41} + \dot{C}_{w,\mathrm{PEM}} + \dot{Z}_{\mathrm{PEM}} = \dot{C}_{42} + \dot{C}_{43}$	$c_{w,\mathrm{PEM}} = c_{w,t,\mathrm{ORC}},\ c_{43} = 0$

To model the multigeneration system, specific input data parameters are selected for simulation. Table 4 presents the input parameters used for system modeling.

Table 4. Parameters for the present study's modeling need to be input [24–27].

Parameters	Unit	Value
T_{eva}	°C	5
T_{cond}	°C	34
T_{abs}	°C	40
T_{gen}	°C	80
P_4	(kPa)	3500
P_6	(kPa)	700
P_{17}	(kPa)	4700
P_{20}	(kPa)	400
$\eta_{t,\text{ORC}}$	–	85
$\eta_{p,\text{ORC}}$	–	85
Collector inlet temperature	°C	100
Solar intensity	W/m^2	850
Width of collector	m	5.76
Length of collector	m	12.27

Table 5 presents a comparison of the operational characteristics of the proposed multigeneration system and lists the related results.

Table 5. The general simulation results for the proposed system.

Parameters	Unit	Value
η_{en}	%	41.58
η_{ex}	%	25.61
$\dot{W}_{t,\text{ORC1}}$	kW	461.9
$\dot{W}_{t,\text{ORC2}}$	kW	227.6
$\dot{W}_{\text{TEG1}}$	kW	138.2
$\dot{W}_{\text{TEG2}}$	kW	328.2
COP_{en}	–	0.8103
COP_{ex}	–	0.3484
Q_{cooling}	kW	1544
$\dot{m}_{\text{H}_2}$	kg/day	493.1
$\dot{\text{E}}\text{x}_{d,\text{tot}}$	kW	55702

The exergy destruction rates for the main parts of the system are depicted in Figure 2. The figure illustrates that the PTC collector and PEM electrolyzer exibits the highest exergy loss rates, respectively. In solar systems, a significant portion of the solar radiation's exergy is transferred to the environment as thermal waste from solar collectors. One contributing factor to the high inefficiency of solar systems is the substantial temperature differential between the fluid entering the panel and its surface temperature.

In Figure 3, the exergy destruction rates within the components of the ORC1 cycle are illustrated. It is evident that the generator, economizer, and TEG unit exhibit the highest exergy destruction rates among these components, all categorized as heat exchangers. Irreversibilities primarily occurin heat exchangers with significant temperature differences between the inlet and outlet streams.

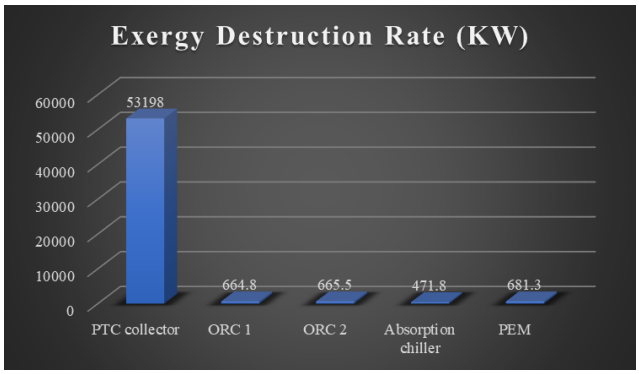

Fig. 2. Rate of exergy destruction for the primary equipment in the system under investigation.

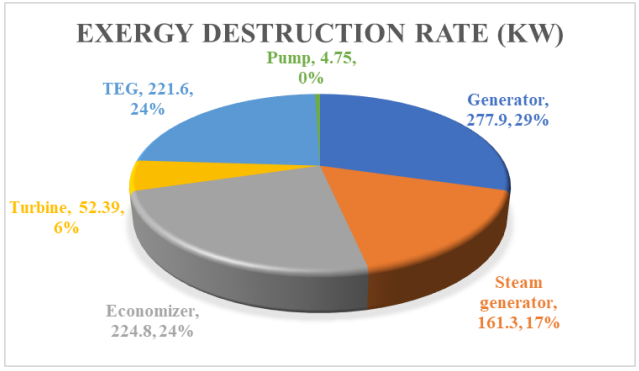

Fig. 3. The exergy destruction rate in the different equipment of the ORC 1.

Figure 4 compares six different ORC cycles applied in the proposed system in terms of overall power generation and hydrogen production rate. The studied working fluids include n-pentane, R245fa, R134a, R236fa and R600. The primary reason for selecting these working fluids is their zero ODP, indicating they are environmentally benign. Table 6 lists some of the thermodynamic properties of these fluids. The results show that among the studied working fluids, R600 achieves the highest power generation of 1159.5 kW and the highest hydrogen generation rate of 494.7 kg/day. Moreover, the lowest level of power and hydrogen output are observed with R245fa working fluid. The power for PEM electrolyzer is entirely supplied by the ORC cycle-generated power, making the selection of a working fluid crucial for maximizing both power and hydrogen production.

Figure 5 illustrates the relationship between the temperature of geothermal water and the rates of power

and hydrogen production. An increase in the geothermal water temperature correlates with higher rates of power and hydrogen production. Elevated geothermal water temperature enhances energy transfer to the ORC 2 cycle, resulting in increased power production in the ORC 2 turbine and TEG. The increased power production of the system results in a higher total power output and a corresponding increase in hydrogen production from the PEM electrolyzer. It is evident that a 50 °C rise in geothermal water temperature causes a 34.5% increase in total power production and a 12.7% increase in hydrogen production. As the geothermal temperature increases from 378 K to 423 K, the power production rate shows a linear progression from 1208 kW to 1625 kW. In contrast, the hydrogen production rate initially decreases from 488.4 kg/day to 475.9 kg/day before increasing to 536.4 kg/day. The turning point for the hydrogen production rate happens around 388 K. It is noteworthy that the hydrogen production pressure is set at 1 atmosphere. The fluctuation in hydrogen production rate is attributed to changes in the mass flow rate of ORC 2, which is not constant and is determined by solving an energy equation in the superheater.

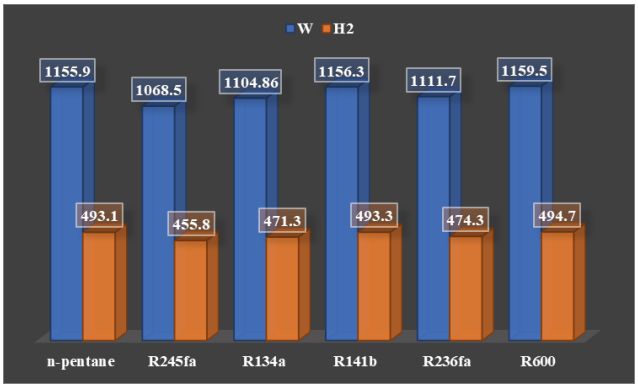

Fig. 4. Comparing various organic Rankine cycle (ORC) working fluids based on their total power output and rate of hydrogen production.

Table 6. Thermodynamic properties of the studied working fluids.

Working fluid	T_c(°C)	P_c (MPa)	ODP	GWP	ASHRAE safety group
n-Pentane	196.55	3.37	0	20	A2
R141b	204.15	4.21	0.086	700	A1
R236fa	125	3.2	0	9810	A1
R134a	122	4.05	0	1430	A1
R245fa	154.01	3.65	0	1030	B1
R600	152	3.79	0	4	A3

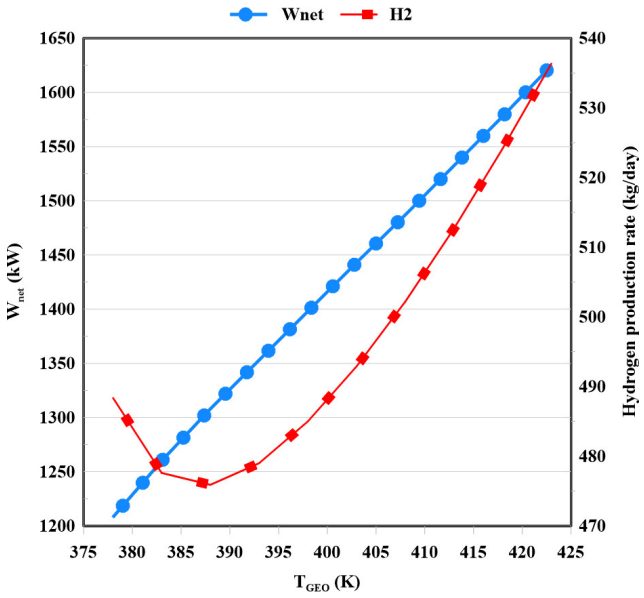

Fig. 5. The temperature of geothermal water influences the production of power and hydrogen.

In Figure 6, the total power and hydrogen production rate are depicted in relation to the collector inlet temperature. According to the data shown, raising the temperature of the solar collector led to a decline in the output variables. This was attributed to a decrease in the initial heat transfer to the sub cycles. During this cycle, a reduction in mass flow rate would result in decreases in both net power and the rate of hydrogen production, resulting in a downward trajectory for the system's output values. For instance, with a change in collector inlet temperature from 353 K to 423 K, the power generated by the system decreases from 1581 kW to 1385 kW, and the rate of hydrogen production decreases from 521.8 kg/day to 480.9 kg/day.

In Figure 7, changes in the collector inlet temperature are shown to affect the exergy efficiency and total cost rate of the system. As the collector inlet temperature increases, the system's exergy efficiency decreases, while the total cost of the system rises. Higher collector inlet temperatures result in reduced power output, leading to lower output values, reduced system efficiency, increased exergy destruction, and consequently, a higher total cost rate.

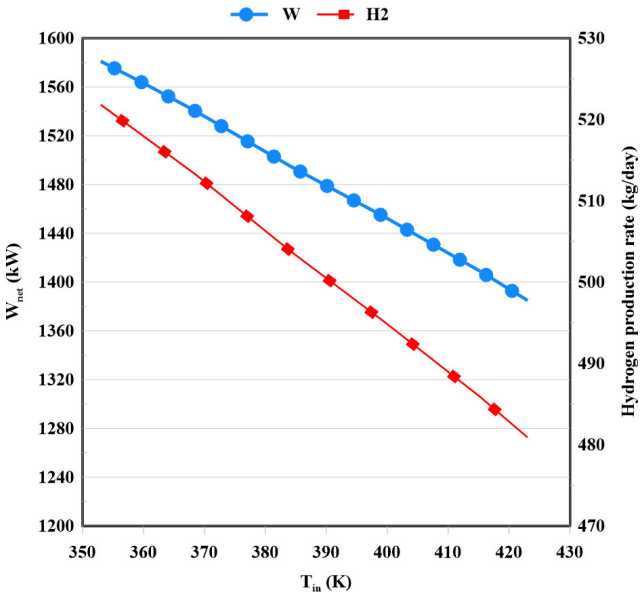

Fig. 6. Effect of collector inlet temperature on the total power and the hydrogen production rate.

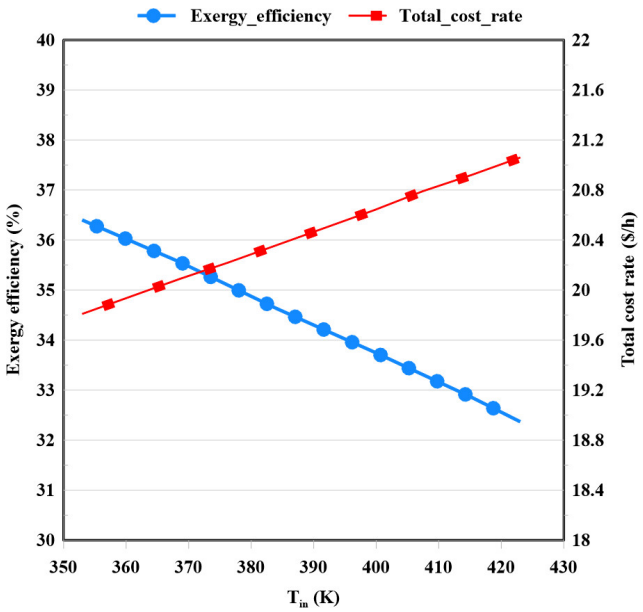

Fig. 7. Impact of the exergy efficiency and total cost rate change with variations in collector inlet temperature.

The turbine inlet temperature is incredibly important. When high-temperature and high-pressure fluids enter the system, it generally leads to an increase in power output. This process involves converting pressure energy into kinetic energy to drive the turbine blades. The changes in thermal efficiency and exergy efficiency due to variations in turbine inlet temperature are illustrated in Figure 8. Converting pressure energy into kinetic energy is necessary to move the turbine blades. In the case of ORC 2, a shift in the temperature at point 4 from 403 K to 503 K results in a 10.7% increase in energetic efficiency and a 20.15% increase in exergetic efficiency. The jump in the figure occurs due to the power production rate generated by the ORC 2 turbine and TEG. Various factors influence the TEG's performance, one of which is its inlet temperature. At approximately 460 K, there is a noticeable increase in the power produced by TEG 2. This increase results from the rise in the TEG's inlet temperature, causing a shift in the graph's trend.

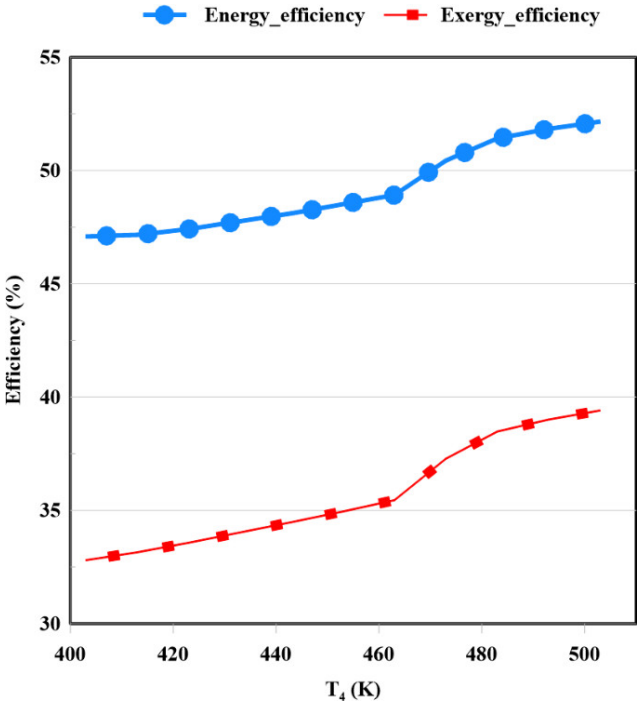

Fig. 8. The effect of changes in thermal efficiency and exergy efficiency due to changes in turbine inlet temperature.

In Figure 9, the impact of adjustments in net power and hydrogen production rate as a result of variations in the ORC 1 turbine inlet temperature is illustrated. According to the charts, elevating the turbine inlet temperature leads to an increase in both total power and hydrogen production rates. When the turbine inlet temperature is raised, a greater amount of energy is transferred to the turbine, consequently allowing for increased power generation by the turbine blades. Moreover, more power is produced in the ORC 1 TEG unit by increasing turbine inlet temperature, which will increase the total power. On the other hand, PEM electrolyzer is completely dependent on the total amount of power produced by the system. Therefore, higher amount of power production by the system will result in the higher amounts of hydrogen produced by the

PEM electrolyzer. The total power output increases from 1308 kW to 1635 kW as the turbine inlet temperature rises from 500 K to 600 K. Additionally, the rate of hydrogen production rises from 468.8 kg/day to 524.5 kg/day during this temperature increase.

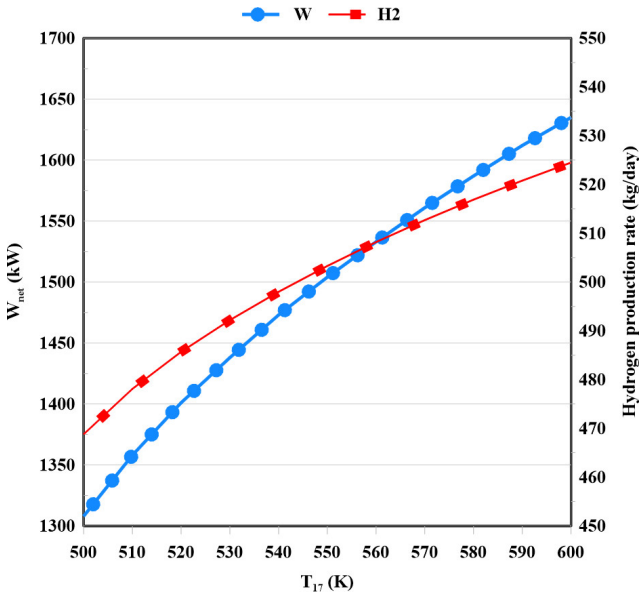

Fig. 9. The effect of changes in net power and hydrogen generation rate due to variation in turbine inlet temperature.

4 Conclusions

Investigations are currently underway to analyze the energy, exergy, and exergoeconomic elements of a multi-generation system powered by solar and geothermal sources. Utilizing EES software, the system is undergoing examination to understand the influence of different parameters on its efficiency. The analysis has revealed that the system boasts an energy efficiency of 41.58% and exergy efficiency of 25.61%. Overall, the system produces a total power output of 1155.9 kW, with the majority being generated by the turbine of ORC 1. Upon examination of the exergy destruction of individual components, it was found that the primary sources of exergy loss are the solar collector, PEM electrolyzer, and ORC 1. Within the ORC 1 cycle, the generator and economizer exhibit the highest rates of exergy destruction.

Among the six different working fluids investigated for the ORC cycles, R600 displays the most advantageous performance for power generation and hydrogen production.

References

[1] Dincer I, Acar C. Smart energy solutions with hydrogen options. International Journal of Hydrogen Energy. 2018;43(18):8579–8599.

[2] Putrus G, Bentley E. Integration of distributed renewable energy systems into the smart grid. Electric Renewable Energy Systems. 2016;p. 487–518.

[3] Zhang T, Yang H. High efficiency plants and building integrated renewable energy systems: Building-integrated photovoltaics (BIPV). Handbook of Energy Efficiency in Buildings: A Life Cycle Approach; Elsevier: Amsterdam, The Netherlands. 2018;p. 441–595.

[4] Dincer I, Acar C. Smart energy systems for a sustainable future. Applied energy. 2017;194:225–235.

[5] Manzano-Agugliaro F, Alcayde A, Montoya FG, Zapata-Sierra A, Gil C. Scientific production of renewable energies worldwide: An overview. Renewable and Sustainable Energy Reviews. 2013;18:134–143.

[6] Tian Y, Zhao CY. A review of solar collectors and thermal energy storage in solar thermal applications. Applied energy. 2013;104:538–553.

[7] Kumar L, Hasanuzzaman M, Rahim N. Global advancement of solar thermal energy technologies for industrial process heat and its future prospects: A review. Energy conversion and management. 2019;195:885–908.

[8] Tashtoush B, Alshare A, Al-Rifai S. Hourly dynamic simulation of solar ejector cooling system using TRNSYS for Jordanian climate. Energy conversion and management. 2015;100:288–299.

[9] Yilmaz F. Thermodynamic performance evaluation of a novel solar energy based multigeneration system. Applied Thermal Engineering. 2018;143:429–437.

[10] Islam S, Dincer I, Yilbas BS. Development, analysis and assessment of solar energy-based multigeneration system with thermoelectric generator. Energy Conversion and Management. 2018;156:746–756.

[11] Colakoglu M, Durmayaz A. Energy, exergy and environmental-based design and multiobjective optimization of a novel solar-driven multigeneration system. Energy Conversion and Management. 2021;227:113603.

[12] Haghghi MA, Holagh SG, Chitsaz A, Parham K. Thermodynamic assessment of a novel multigeneration solid oxide fuel cell-based system for production of electrical power, cooling, fresh water, and hydrogen. Energy conversion and management. 2019;197:111895.

[13] Cioccolanti L, Hamedani SR, Villarini M. Environmental and energy assessment of a small-scale solar Organic Rankine Cycle trigeneration system based on Compound Parabolic Collectors. Energy Conversion and Management. 2019;198:111829.

[14] Saleem MS, Abas N, Kalair AR, Rauf S, Haider A, Tahir MS, et al. Design and optimization of hybrid solar-hydrogen generation system using TRNSYS. International Journal of Hydrogen Energy. 2020;45(32):15814–15830.

[15] Uche J, Muzás A, Acevedo L, Usón S, Martínez A, Bayod A. Experimental tests to validate the simulation model of a Domestic Trigeneration Scheme with hybrid RESs and Desalting Techniques. Renewable Energy. 2020;155:407–419.

[16] Sohani A, Delfani F, Hosseini M, Sayyaadi H, Karimi N, Li LK, et al. Dynamic multi-objective optimization applied to a solar-geothermal multigeneration system for hydrogen production, desalination, and energy storage. International Journal of Hydrogen Energy. 2022;47(74):31730–31741.

[17] Cengel YA, Boles M, Kanoglu M. Thermodynamics: an engineering approach. McGraw-Hill; 2011.

[18] Mokhtari H, Esmaieli A, Hajabdollahi H. Thermoeconomic analysis and multiobjective optimization of dual pressure combined cycle power plant with supplementary firing. Heat Transfer—Asian Research. 2016;45(1):59–84.

[19] Khanmohammadi S, Atashkari K, Kouhikamali R. Exergoeconomic multi-objective optimization of an externally fired gas turbine integrated with a biomass gasifier. Applied Thermal Engineering. 2015;91:848–859.

[20] Din I, Rosen MA, Ahmadi P, et al. Optimization of energy systems. John Wiley & Sons; 2017.

[21] Rostamzadeh H, Namin AS, Ghaebi H, Amidpour M. Performance assessment and optimization of a humidification dehumidification (HDH) system driven by absorption-compression heat pump cycle. Desalination. 2018;447:84–101.

[22] Al-Alili A, Hwang Y, Radermacher R, Kubo I. A high efficiency solar air conditioner using concentrating photovoltaic/thermal collectors. Applied Energy. 2012;93:138–147.

[23] Mahmoudan A, Esmaeilion F, Hoseinzadeh S, Soltani M, Ahmadi P, Rosen M. A geothermal and solar-based multigeneration system integrated with a TEG unit: Development, 3E analyses, and multi-objective optimization. Applied Energy. 2022;308:118399.

[24] Al-Sulaiman FA. Exergy analysis of parabolic trough solar collectors integrated with combined steam and organic Rankine cycles. Energy Conversion and Management. 2014;77:441–449.

[25] Mohammadi M, Mahmoudan A, Nojedehi P, Hoseinzadeh S, Fathali M, Garcia DA. Thermoeconomic assessment and optimization of a multigeneration system powered by geothermal and solar energy. Applied Thermal Engineering. 2023;230:120656.

[26] Tekkanat B, Yuksel YE, Ozturk M. The evaluation of hydrogen production via a geothermal-based multigeneration system with 3E analysis and multi-objective optimization. International Journal of Hydrogen Energy. 2023;48(22):8002–8021.

[27] Panahi Zadeh F, Bozorgan N. The energy and exergy analysis of single effect absorption chiller. International Journal of Advanced Design and Manufacturing Technology. 2011;4(4).